Ph. Baidoo[*]
Instructor

M. Amoah[†]
Associate Professor

J. Acheampong[‡]
Instructor

Tensile Properties and Fatigue Behavior of AHSS-DP 350/600 Subjected to Laser Shock Processing

This work presents the effects of strain rate on the tensile properties and fracture morphologies of AHSS-DP 350/600 subjected to LSP. Fatigue crack growth test was performed to evaluate fatigue behavior in the metallic plate of AHSS-DP350/600. However, this material is used in automobile industry and enhancing it fatigue resistance is a challenge in material engineering. In order to evaluate and compare the influence of the microstructure on their mechanical and chemical properties, tensile and hardness test were performed and analysis. This revealed that the LSPed specimens have higher values of yield stress, maximal stress, Young's modulus than non-LSP specimens, the elongation and hardness as a result of their porosity and pore size influenced. It was observed that the macroscopic (tensile tests) and microscopic (microhardness tests) properties of the non-LSP are sensitive to these defects generated during the material machining process and LSP specimens could prolong the material working life.

Keywords: AHSS-DP350/600; Laser peening; Tensile-fracture; Fatigue crack growth; Micro-hardness

1 Introduction

Advance higher strengthen steel dumping 350/600 (AHSS-DP 350/600) particularly , usually have excellent corrosion resistance, good weldability and formability, good resistance to hydrogen embrittlement, in addition to high ductility and toughness. However, they have relatively low yield strength in the annealed state [1]. There are various strengthening mechanisms for AHSS-DP 350/600, such as grain refining, transformation strengthening and work hardening, converting them in materials widely used in engineering applications, such as in the manufacturing, nuclear, chemical, oil and petrochemical, and food industries, as well as the medical industry for biomedical implants [2,3]. Recently there has been an enormous amount of research addressing the improvement of the mechanical properties of austenitic stainless steel [4,5,6,7,8] without lowering corrosion resistance [9,10,11,12].

[*] Instructor, Department of Mechanical &Automotive Engineering, University of Education, P. O. Box 25, Winneba, Ghana Mypennich@yahoo.com
[†] Associate Professor, Department of Mechanical &Automotive Engineering, University of Education, P. O. Box 25, Winneba, Ghana akwasiamponsah07@gmail.com
[‡] Instructor, Department of Mechanical &Automotive Engineering, University of Education, P. O. Box 25, Winneba, Ghana prosperah@yahoo.com
Receive : 2019/01/10 Accepted : 2019/02/15

AHSS-DP 350/600 are highly used by hot-rolling, followed by cold-swaging and annealing processes. The application fields of AHSS-DP 350/600 are the Automobile and shipment industry. Fracture of metallic filaments differs in many respects from fracture of AHSS-DP 350/600 samples. Particular manufacturing processes. So far, a few research efforts have been performed on the comparison of the mechanical and microstructural properties of AHSS-DP 350/600 using difference energy of density levels and a squared (4*4) mm spot-pulse LSP. Measurement of mechanical properties is a major part of the domain of materials characterization, therefore, in the present work, the mechanical properties and microstructural features of an AHSS-DP 350/600 stainless steel with and without LSP, were systematically studied in order to establish the relationship between the microstructure and the mechanical properties. It is noteworthy that the AHSS-DP 350/600 were tested individually in a capable of conducting tensile, hardness and morphology on every specimens on NOLSP, S25J and S30J samples however, benefits offered by LSP have been revealed in AHSS-DP 350/600.

2 Experimental procedures

2.1 Material and sample preparation

The automobile , transportation industry now highly uses AHSS-DP 350/600 plates which have a good low temperature impact, homogeneous microstructure, good cool forming performance, low ductile-brittle transition and finally good resister to corrosion. AHSS-DP 350/600 is used under harsh environment of automotive industries and transportation platforms. The chemical composition and mechanical properties of AHSS- DP350/600 are shown in Table (1) and (2).

Table 1 Mechanical properties of AHSS-DP350/600

Steel Grade	YS (MPa)	UTS (MPa)	Total EL(%)	N-Value (5-15%)	R-Bar	K-Value (MPa)	Application Code
DP350/600	350	600	24-30	0.14	1	976	A,C,F

Source: *www.autosteel.org.*

Table 2 Chemical properties of AHSS-DP350/600

Material	C	Mn	P	S	Si	Cn	Sn	Ni
DP350/600	0.102	1.574	0.013	0.003	0.087	0.025	0.013	0.02

Source: www.autosteel.org

Table 3 LSP parameters of AHSS-DP350/600

Sample No:	Terms	Impact times	laser energy (J)	Pulse width (ns)	Spot diameter ($mm^{2)}$	Spot spacing (mm)	Confining layer	Absorbing layer	laser density (gw/cm^2)
1.	NO LSP	NO LSP	NIL	NIL	NIL	NIL	NIL	NIL	NIL
2.	S30J	Single	30	15	4*4	3.4	water	Al foil	12.5
3.	S25J	Single	25	15	4*4	3.4	water	Al foil	10.4

Improving of fatigue property of AHSS-DP 350/600 plays a pivotal role in prolonging material service life, and LSP is a novel anti-fatigue technology for a betterment expansion of metal life span and periodic cycles. According to GB/T6398-2000 standard and experimental conditions on the dog bone specimens are prepared with the dimensions shown in Figure (1), to do reconnoiter on the effect of LSP on the FCG rate on AHSS-DP 350/600. The positions of the LSP zone, for AHSS-DP 350/600 were carefully marked by marking pen input to distinguish from different zones treatment.
The dog bone samples/specimens prepared procedures are shown as follows:

1. Cutting specimens at stated dimensions by electro-discharge machined (EDM);
2. Grinding and polishing samples with SiC paper at different grades of roughness;
3. Cleaning samples in deionized water and saving in drying box;
4. Eliminating machined surface residual stress of dog bone specimens by naturally aging treatment for a particular interval of time.

2.2 Principle of LSP and experimental parameters

The laser shock peening (LSP) utilized a heavy energy laser pulses to hit the outer body layer of material and then formed plasma. The restrained plasma created a high surface pressure propagating into the material as a shock wave. When the pressure of shock wave exceeded the dynamic yield strength of the material, it produced a change of plastic state in the near-outward body layer of the metal. This adopted LSP principle is schematically shown in Figure (2). The massive LSP impacts in the treated zone of the dog bone of AHSS-DP 350/600 were carried out using a Q-switched Nd: YAG (Neodymium doped Yttrium Aluminum Garnet) laser system and a numerical control workbench. Shock was done on specimens.

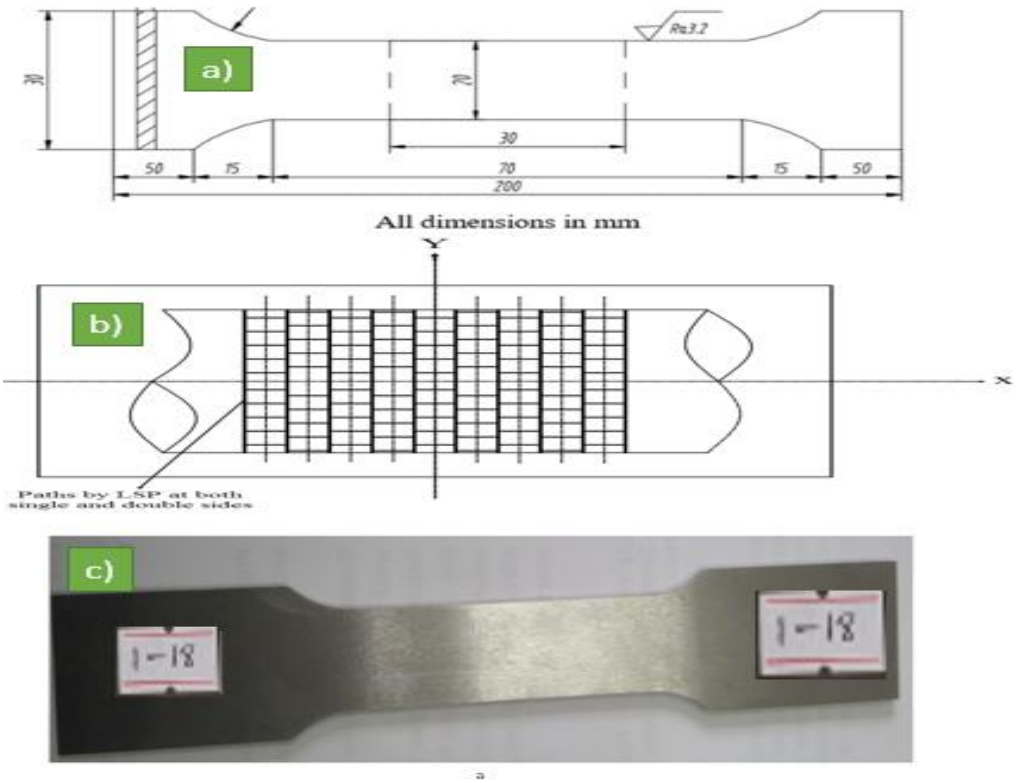

Figure 1 a) Specimen drawn dimensions, b) LSP paths and c) picture

All samples were sunk into a water bath when they were processed by LSP. A water layer with a thickness of about 1mm was used as the transparent confining layer and the professional aluminum foil with a thickness of 0.1mm was used as an absorbing layer to protect the sample surface from the thermal effect.

2.3 Tensile Properties under different density

The tensile sample was cut into the dog-bone shaped tensile sample as said above in the dimensions shown in Figure (1) and table (3) gave the LSP parameters of AHSS-DP 350/600. Figure 3.a) the dimensions of the tensile sample subjected to LSP and non-LSP, 3.b) was sample of one sided shocked energy of 30J and density of 12.5 gw/cm^{2,}, 3.c) one sided shocked energy of 25J and density of 10.4 gw/cm^2 and all used square spot of 4*4 mm^2 pulse
as against non- LSP in figure 3.d). From Figure (3) again, after the necessary set up was done on tensile test, it can be seen that "stress" on the specimens increases until it reached a maximum applied stress, while the specimens deforms or changes shape uniformly along the entire gauge length. This points could determine the tensile strength or maximum stress (or load) the material can support at a particular point in time, observed by a noticeable “necking” or reduction in the breaks or fails as indicated.

2.4 Rockwell hardness test

This methodological test is among the effective and efficient indentation hardness tests used today. Most of this kind of test, however measure the deformation that happens when the material under test is penetrated with a specific type of indenter. Therefore, the different levels of force are applied to the indenter at specified rates of two different points and with specific dwell times. The Rockwell hardness of the material is based on the difference in the deeper inner sizes of the indenter at two periodic of times during the testing cycle. The value of hardness is measured using a formula that was derived constant to yield a number falling within an arbitrarily defined range of numbers known as a Rockwell hardness scale.

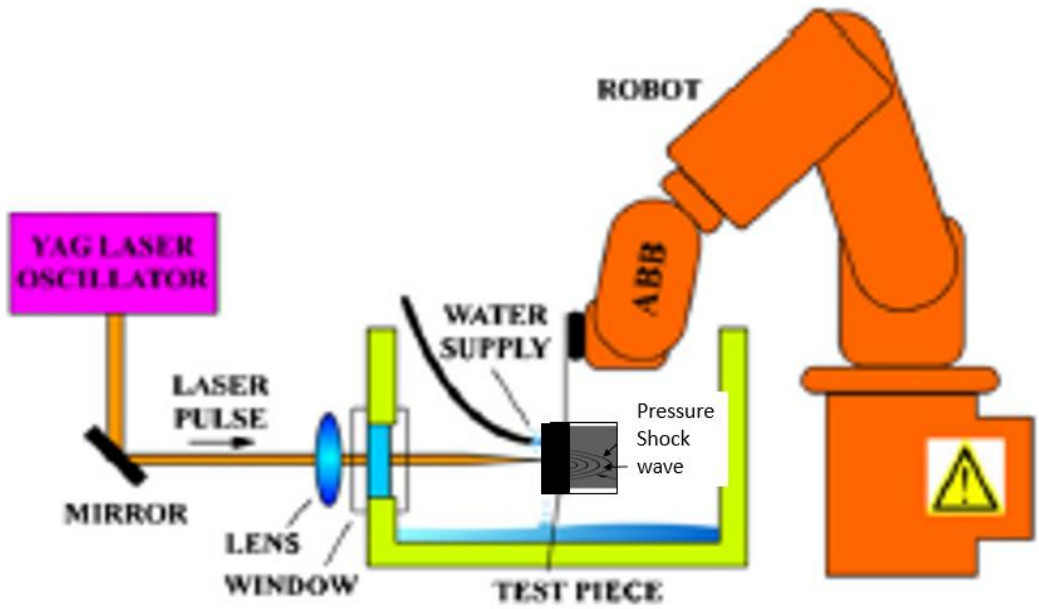

Figure 2 Schematic principle of LSP

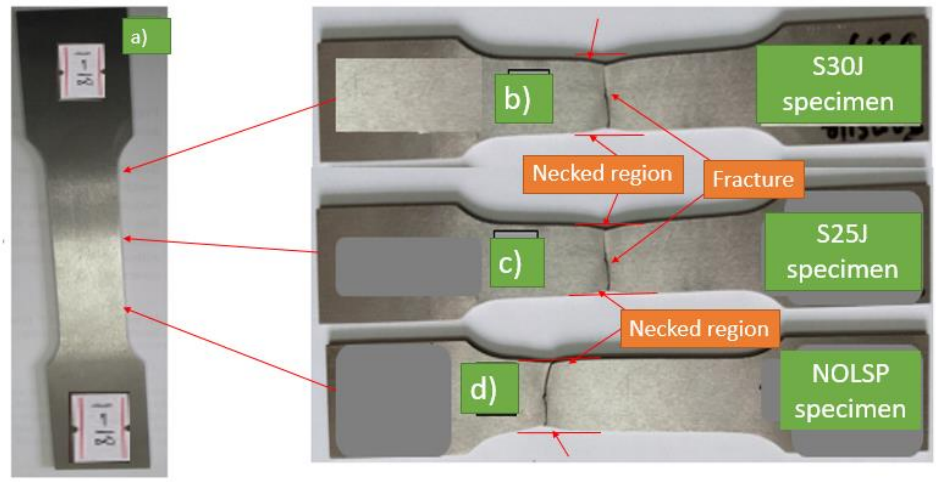

Figure 3 shown both treated and non-treated LSP specimens after tensile test: a) before tensile test and b), c), and d) after tensile tested.

The indenter is brought into contact with the material to be tested, and an initial load of force is applied to the indenter. The initial force is usually held constant for an amount of time (dwell time), besides the depth of indentation is measured. After the measurement is done more force is applied at a rate of a period to increase the applied force to maximize the increment as the major load. The force is held fixed for a particular interval of time, after that the additional force is taken out which returning to the previous force level.
In this paper hardness measurement and force of 150gf was applied for 10s.

2.5 XRD test

The X-ray diffraction (XRD) pattern of the specimens were recorded with Cu-Kα radiation at a frequency of $\lambda = 1.5406$ Å within a range of 2Θ from 5° to 30° at a speed of 5°/min. It can be seen from the result of the microstructural examination that, the high pressure shockwave caused the plastic deformation and refinement of grains. In this study the effect of LSP on the AHSS-DP 350/600, the XRD method was used to analyze the various diffraction patterns by the untreated and treated LSP energies; S25J and S30J specimens. From figure (6) shows the XRD patterns of specimens treated and untreated.

2.6 Fracture morphologies observation

The fracture end of the bracken specimen's surface were cleaned after the fatigue cycle test and kept for normal dried system and therefore studied them very carefully. However the fracture surfaces were observed by scanning electron microscopy (SEM, JSM-6490LV).

3 Results and Discussion

3.1 Tensile Tests

The engineering stress-strain curves of both non-LSP and LSP specimens are shown in figure (4). It can be seen that the non-LSP samples show lower tensile mechanical properties than those of the LSPed specimens; the results were summarized in figure (4).

The parabolic shape of the LSPed specimens curve indicates that strain hardening occurs throughout the duration of the stress application, but such an amount of strain hardening for a given increment of stress decreases as stress increases. Concerning the non-LSP, instead of a parabolic-shaped curve, the stress increased monotonically up to failure, which means that there was a strain hardening of the non-LSP structure. It was clear that the LSPed mechanical properties exceed those of the non-treated. An improvement of yield stress (σ_y) and Young's modulus € in the non-LSP was expected due to grain refinement in comparison to the LSPed specimens, however the result was opposite to that expected.
During cold-work crystalline defects like dislocations and porosity increase with the degree of deformation and decrease the mechanical properties. In addition, the sample sizes for non-LSP and LSP affect the results of mechanical tests due to well compressive stress distribution of the LSPed specimens. The coupled effect of crystalline defects and tested area size of samples were evident in the reduction of mechanical properties of non- LSP evaluated in macro-scale in comparison to the LSP specimens in figure (4).

3.2 Micro hardness

Rockwell hardnesstests were conducted in both kinds of samples; the results are presented in figure (5), which shows that the hardness of the LSPed samples of S30J was higher and followed by S25J than that of NOLSP specimen. This lower microhardness of NOLSP specimen could be due to their higher porosity; that is why nan indentation measurements on cross-section were performed in order to determine hardness and Young's modulus of both LSP and non-LSP specimens. Regarding hardness measurements by nanindentation, the LSPed of both material of S30J and S25J presented a value of 72.0 HRB and 71.0 HRB, while the NOLSP presented a value of 69.0 HRB; in both cases these results were significantly greater than those reported from the manufacture respectively. This can be explained by the fact that the nanindentation measurements were carried out in flaw-free small regions, namely porosity-free, while Rockwell hardnessmeasurements were performed over large regions that might contain porosity.

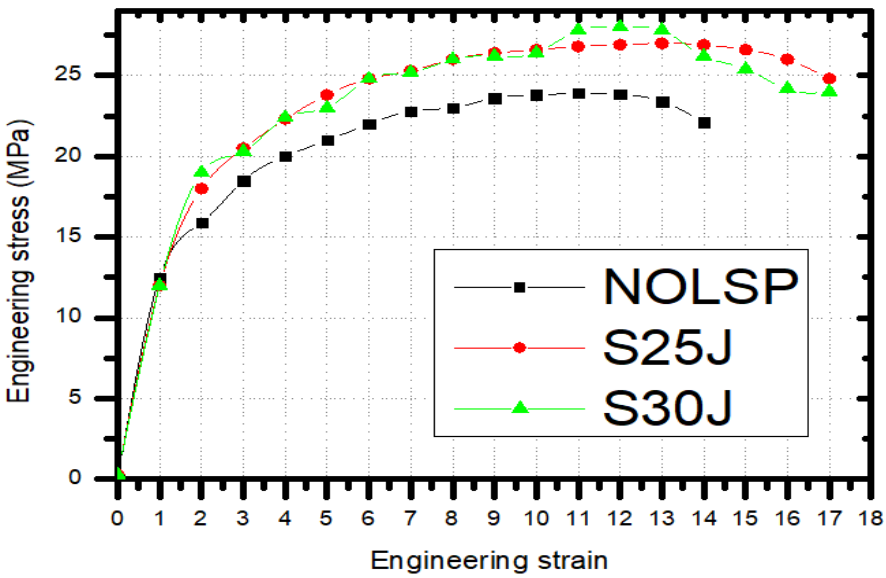

Figure 4 shown tensile stress of engineering stress and engineering strain

In reference to the Young's modulus, the values found by nan indentation for the LSPed specimens were respectively close to that reported for the AHSS-DP 350/600 in table (2), According to Young's modulus results obtained by tensile tests and nan indentation. The values for LSP material were similar by both techniques, but in the case of non-LSP, the value is less for tensile tests as shown in figure (5). This difference can be again explained by the large number of flaws that samples contain throughout their longitudinal section, especially in the case of non-LSP. The hardness and the Young's modulus measured by nanoindentation are higher because the measurements were performed over defect-free areas. The higher values in non-LSP properties measured by nanoindentation yield evidence that deformation of non-LSP during cold-work induces greater material strengthening, making it stiffer by reducing their deformation ability without reaching a completely brittle material.

3.3 XRD diffraction and phase analysis

XRD patterns of the studied samples plotted in 6, it was revealed that no new peaks were formed after series of shocks on the specimens. It was again observed that there was no phase transformation in the surface layer of the AHSS-DP 350/600 by LSP. However it could observed that the diffraction peaks of the treated specimens were broader than that of untreated, indicated that refined grains, to dislocation caused as a results of high plastic strain deformation and micro-strain among adjacent peaks, an increment in micro-strian in the surface layer of the and/or increament in the crystaal lattice distortion. [13] a result of the dislocation multiplication after LSP. The atomic distance s were altered as a result of the high strain plastic deformation by higher shocked of S30J. The average grain size was determined from the full width at half maximum (TWHM) of Bragg diffraction peaks via standard Scherre - Wilson and equation and miller indices; [14] (Eq. 1).

$$\mathrm{FWHM} \times \cos\theta = K \times \lambda / D + 4 \times \epsilon \times \sin\theta \quad (1)$$

Where D is the crystallite size, K is the shape factor of the lattice constant (K = 0.94), λ is the wavelength of the X ray (λ = 1.5418Å), ε is the microstrain and θ, the Bragg angle.

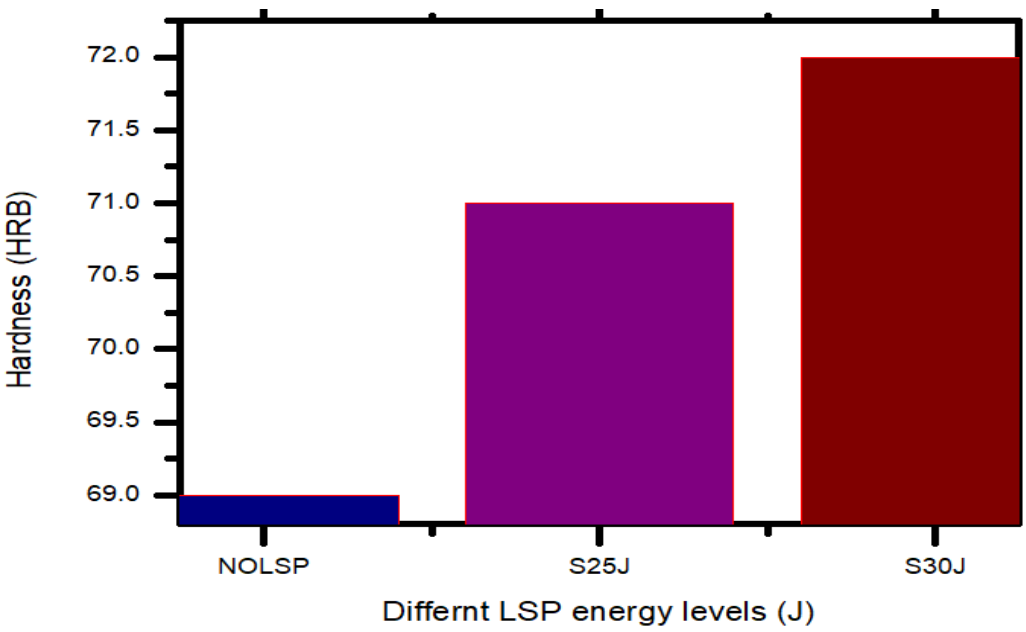

Figure 5 shown the Rockwell hardness results of specimens

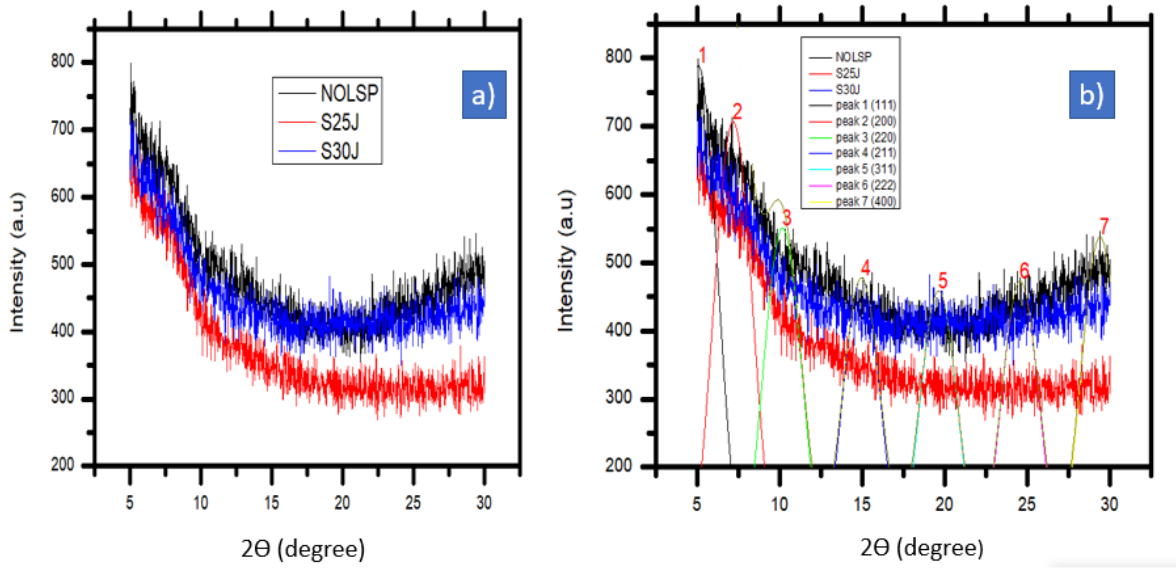

Figure 6 XRD patterns analysis of with and without LSP samples.(a) Indexed graph and (b) Magnified graph

From figure (7) it revealed that both treated and untreated LSP samples have the same crystalline structure but the FWHM, Crystallite size, micro strain and dislocation density were differed. As the energy increases from S25J to S30J average grain size decreases, but the micro-strain increased by the shocked. During plastic deformation of austenitic stainless steels at room temperature, the martensitic transformation occurs from the austenite phase. The structure observed in the diffraction peaks consists of a mixture of chemical composite passes of AHSS-DP 350/600. Which corresponds and characteristic of martensite and austenite phases, respectively.

However, the XRD patterns of AHSS-DP 350/600 samples in different states present a remarkable difference in intensity. The peaks of the treated sample are sharp, while the peaks of the untreated pattern exhibit a significant shortening that indicates a crystal size refinement. The grain refinement could be attributed to the high strains during plastic deformation induced by LSP contributed to the generation of dislocation lines [15]. The figure also shown that FWHM of (111) (200) (220) (211) (311) (222) and (400) peak increased more after the treatment as against non-treated.

3.4 Morphology observation

The tensile fracture morphology of the samples was analyzed by optical microscopy in figure (6). The necking and neck propagation were observed for all specimens, which are associated with ductile materials in figure (3). And table (2) showed the mechanical properties of AHSS-DP 350/600 samples. Ductile fractures are characterized by tearing of metal along with appreciable gross plastic deformation. Ductile tensile fractures in most materials have a gray and fibrous appearance [16]. The quantity and size of pores after tensile tests can be seen in figure (6), respectively for treated and non-treated specimens; in the case of non-LSP, the fracture surface contains many structure of adjoining cavities like deep dimples, distributed homogeneously throughout the maximum surface.

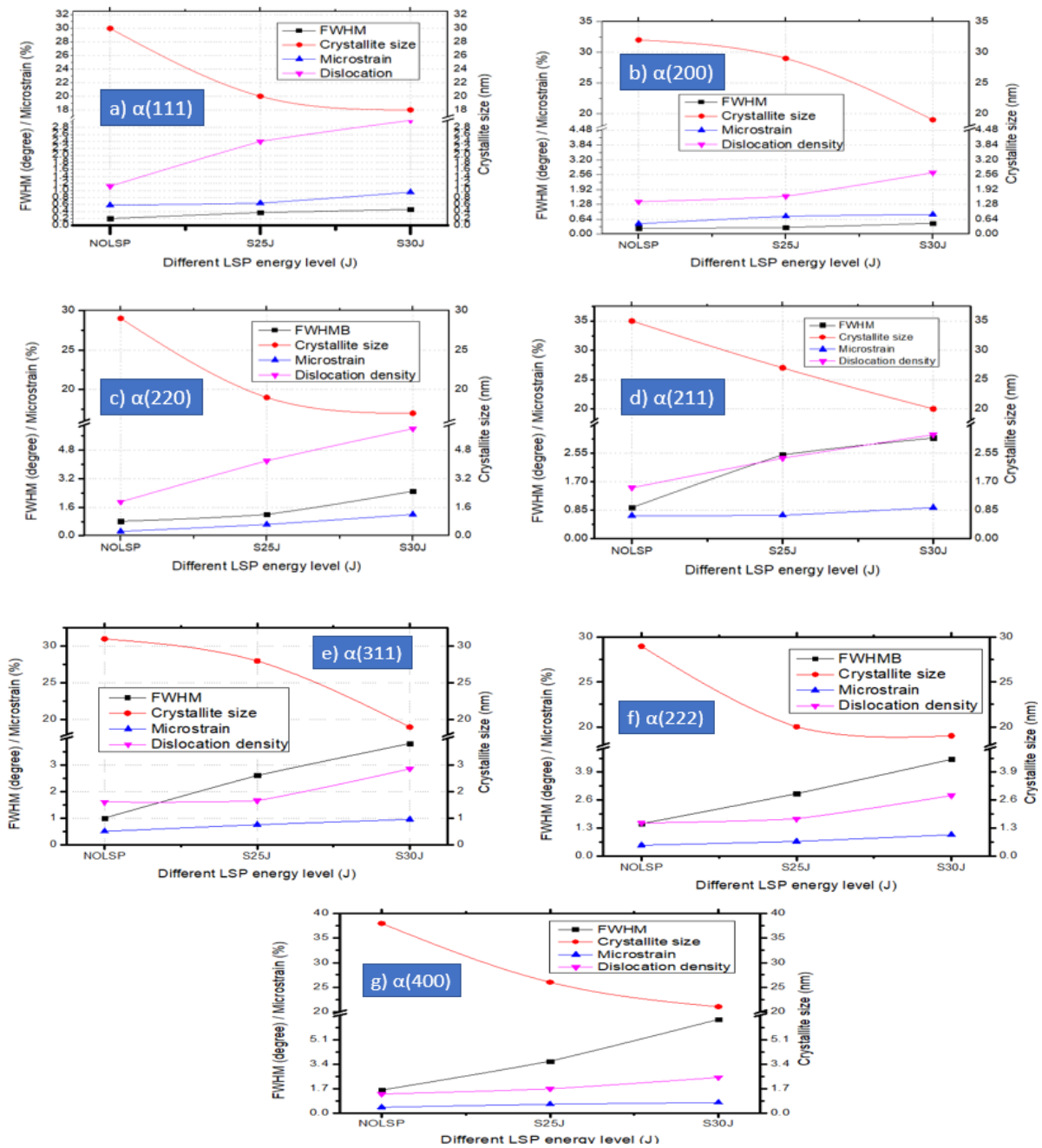

Figure 7 FWHM, microstrain, crystallite size, dislocation density of AHSS-DP 350/600.

The below fractographic examinations of the broken tensile samples reveals characteristic features like dimple coalescence and fatigue crack indication of ductile failure at non- shocked density rates, and the dimple coalescence takes place in parts containing inclusions or precipitates. It is well known that the presence of impure LSP particles restricts dislocation mobility and has an obvious attribution to the initiation of crack nucleus and crack propagation. Moreover, the presence of dimple coalescence indicates clearly a trans-granular ductile-mode fracture, and the dimple size in the fracture surface is a function of fatigue life, which has a direct relation with the shocked density. [17]. The geometry of dimple and its correlation with mechanical properties in the structural materials have been investigated [17], and the results indicated that there was a systematic correlation between mechanical properties and the dimple size at ductile fracture with the shocked density variation.

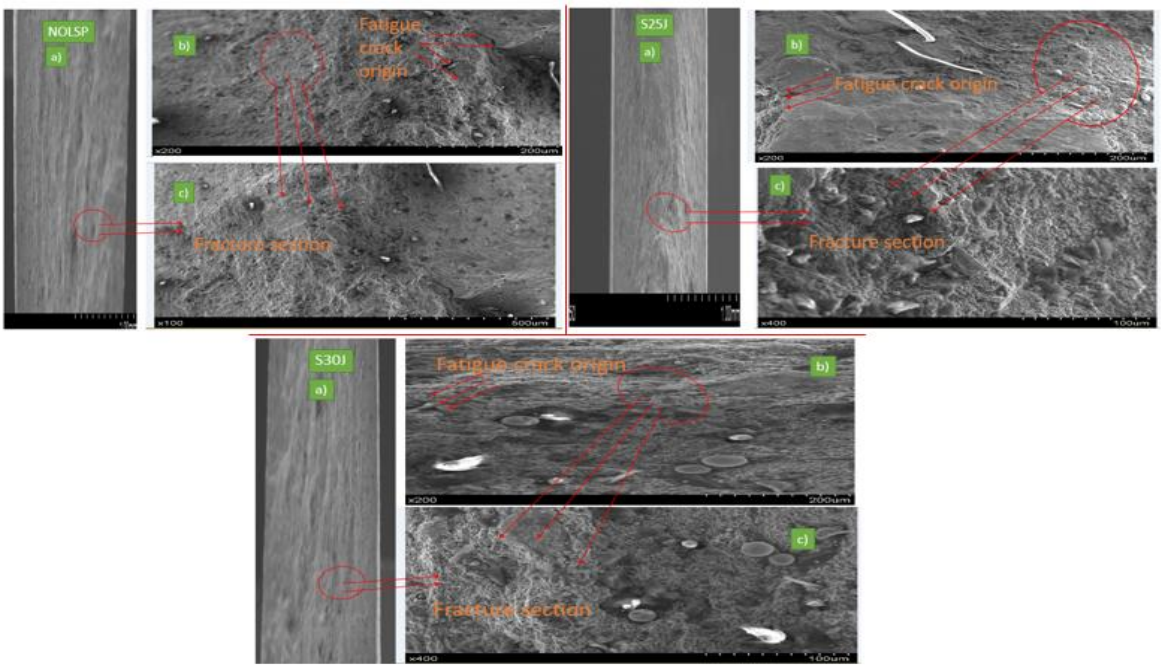

Figure 8 Fracture surface morphologies of tensile tested specimens: **a**) NOLSP **b**) S25J and **c**) S30J

From figure (6), it can be concluded that there were obvious differences in the dimple size at different shocked spots of density and energy pulse, and the dimple size showed a notable shocked spot energy rate sensitivity after LSP. With the increment of the shocked density, the dimple size and the dimple depth increase, and when the shocked density increases from 10.5wg/cm^2 to 12.4wg/cm^2 as showed in table (3), there was the dimple coalescence morphology on the fracture surfaces, and dimple becomes gradually larger and deeper. Hence, it is reasonable to estimate the mechanical properties of AHHSS-DP 350/600 with different shocked density after LSP through fracture surface analysis of the dimple and fatigue crack regions. However, it should be mentioned that if fracture morphology of a sample without LSP are given by comparison, it will provide more evidence to explain that LSP give a strong impact on the higher shocked density sensitivity of AHSS-DP 350/600.

4 Conclusions

In this work tensile, microhardness and nanoindentation tests were done on an AHSS-DP 350/600 steel in the LSP and non-LSP specimens, in order to evaluate and compare the influence of the microstructure on their mechanical and chemical properties. Both presentations showed a similar microstructure and tensile fracture morphology. Tensile and hardness tests showed that the LSPed specimens have higher values of yield stress, maximal stress, Young's modulus than non-LSP specimens, elongation and hardness, as a result of their porosity and pore size. It was observed that the macroscopic (tensile tests) and microscopic (microhardness tests) properties of the non-LSP are sensitive to these defects generated during the material machining process and LSP specimens could prolong the material working life. Throughout nanoindentation testing a very small volume of material could be tested. The superior mechanical properties of treated and non-treated obtained by nanoindentation, in comparison with those obtained by tensile tests and microhardness, are due to the capability of nanoindentation of performing measurements on a small and porosity-free area. With this technique, higher values of hardness and Young's modulus on non-treated specimen were reached in comparison to treated specimen's condition. These results were expected due to the greater plastic deformation induced in non-LSP during their processing.

Author Contributions: Philip Baidoo designed the experiments with Martin Amoah; all authors performed the experiments, analyzed the data and discussed the results; Philip Baidoo and Martin Amoah contributed with reagents/materials/analysis tools; Philip Baidoo wrote the paper; martin Amoah and Juliet Acheampong revised the paper.

Conflicts of Interest: The authors declare no conflict of interest.

References

[1] Davis, J.R., "*Stainless Steel. In ASM Specialty Handbook"*, 1st Ed. ASM International, Northeast, OH, USA, (1994).

[2] Lanzillotto, C.A.N., and Pickering, F.B., "Structure-property Relationships in Dual-phase Steels", Met. Sci., Vol. 16, pp. 371-382, (1982).

[3] Baek, J.H., Kim, Y.P., Kim, W.S., and Kho, Y.T., "Effect of Temperature on the Charpy Impact and CTOD Values of Type 304 Stainless Steel Pipeline for LNG Transmission", KSME Int. J., Vol. 16, 351-357, (2002).

[4] Hedayati, A., Najafizadeh, A., Kermanpur, A., and Forouzan, F., "The Effect of Cold Rolling Regime on Microstructure and Mechanical Properties of AISI 304L Stainless Steel", J. Mater. Process. Tech., Vol. 210, pp. 1017-1022, (2010).

[5] Chen, T.C., Chen, S.T., and Tsay, L.W., "The Role of Induced α-martensite on the Hydrogen-assisted Fatigue Crack Growth of Austenitic Stainless Steels", Int. J. Hydrog. Energy, Vol. 39, pp. 10293-10302, (2014).

[6] Dehsorkhi, R.N., Sabooni, S., Karimzadeh, F., Rezaeian, A., and Enayati, M.H., "The Effect of Grain Size and Martensitic Transformation on the Wear Behavior of AISI 304L Stainless Steel", Mater. Des., In Press, (2014).

[7] Switzner, N.T., Van Tyne, C.J., and Mataya, M.C., "Effect of Forging Strain Rate and Deformation Temperature on the Mechanical Properties of Warm-worked 304L Stainless Steel", J. Mater. Process. Tech., Vol. 210, pp. 998-1007, (2010).

[8] Weber, S., Martin, M., and Theisen, W., "Impact of Heat Treatment on the Mechanical Properties of AISI 304L Austenitic Stainless Steel in High-pressure Hydrogen Gas", J. Mater. Sci., Vol. 47, pp. 6095-6107, (2012).

[9] Bai, T., Chen, P., and Guan, K., "Evaluation of Stress Corrosion Cracking Susceptibility of Stainless Steel 304L with Surface Nano Crystallization by Small punch Test", Mater. Sci. Eng. A Struct., Vol. 561, pp. 498–506, (2013).

[10] Bai, T., and Guan, K., "Evaluation of Stress Corrosion Cracking Susceptibility of Nano Crystallized Stainless Steel 304L Welded Joint by Small Punch Test", Mater. Des, Vol. 52, pp. 849-860, (2013).

[11] Roffey, P., and Davies, E.H., "The Generation of Corrosion under Insulation and Stress Corrosion Cracking Due to Sulphide Stress Cracking in an Austenitic Stainless Steel Hydrocarbon Gas Pipeline", Eng. Fail. Anal., Vol. 44, pp. 148-157, (2014).

[12] Li, W.J., Young, M.C., Lai, C.L., Kai, W., and Tsay, L.W., "The Effects of Rolling and Sensitization Treatments on the Stress Corrosion Cracking of 304L Stainless Steel in Salt-spray Environment", Corros. Sci., Vol. 68, pp. 25-33, (2013).

[13] Roland, T., Retraint, D., Lu, Ke., and Lu, J., "Enhanced Mechanical Behavior of a Nano Crystallised Stainless Steel and its Thermal Stability", Material Science and Engineering: A., Vol. 445, pp. 281-288, (2007).

[14] Williamson, G., and Hall, W., "X-ray Line Broadening from Filed Aluminum and Wolfram", Actametallurgrica, Vol. 1, Issue. 1, pp. 22-31, (1953).

[15] Lu, J.Z., Lou, K.Y., Zhang, Y.K., Cui, C.Y., Sun, G.F., Zhou, J.Z., Zhang, L., You, J., Chen, K.M., and Zhong, J.W., "Grain Refinement of LY2 Aluminum Alloy Induced by Ultra-high Plastic Strain during Multiple Laser Shock Processing Impacts", Actamaterialia, Vol. 58, No. 11, pp. 3984-3994, (2010).

[16] Garcia–Bernal, M. A., Mishra, R. S., Verma, R., and Hernandez-Silva, D., "High Strain Rate Superplasticity in Continuous Cast Al-Mg Alloys Prepared via Friction Stir Processing", Scripta. Materialia, Vol. 60, No. 10, pp. 850-853, (2009).

[17] Arpan, D., and Soumitra, T., "Geometry of Dimples and its Correlation with Mechanical Properties in Austenitic Stainless Steel", Scripta Materials, Vol. 59, No. 9, pp. 1014-1017, (2008).